nature astronomy

Supplementary information https://doi.org/10.1038/s41550-025-02729-x

Electrical conductivities of (Mg,Fe)O at extreme pressures and implications for planetary magma oceans

In the format provided by the authors and unedited

Supplementary materials

Contents

1 Synthesis of (Mg,Fe)O targets

Fe was diffused into single-crystal MgO (periclase) samples in order to produce various (Mg,Fe)O compositions. Both reagent grade MgO nanopowder and MgO rod shavings (both greater than 99 percent) served as the source MgO powder. The powder was dehydrated in a platinum crucible and muffle furnace at 500 C for 3 hours, weighed while still hot, and then added to an agate mortar. Reagent grade Fe(II)O (greater than 99.5 percent) was then added to the mortar to create a mix of ~ 1.5 g. Each mix was homogenized by grinding with an agate pestle under ethanol, twice for 15-30 minutes. Two different mixes were created, targeting two different molar concentrations of Fe and Mg (Supplementary Table 1). The mixes were then pelletized using a 10-ton press held at 5000 psi for approximately 1 hour. Pellets and pellet fragments were placed into individual quartz tubes and torch-sealed under vacuum between 2.0×10^{-2} and 4.0×10^{-2} mbar. Reaction of the MgO-FeO powders was performed by heating the sealed quartz tubes in a 1-bar furnace at ≈ 1200 C for 66 hours.

After this reaction step, the pelletized pieces were removed from the tubes and crushed into a powder that served as the homogenized source material for the final Fe-diffusion experiments. For this last step, a single-crystal periclase square was embedded between two compacted layers of the desired Mg-Fe concentration powder in another quartz tube, and a cylindrical quartz plug rested on top of this assemblage to prevent powder from climbing up the glass vessel during evacuation. The tubes were evacuated to between 2.0×10^{-2} and 4.0×10^{-2} mbar and torched-sealed in the same manner as before, and heated in a muffle furnace at 1090 C for 309 hrs after which power to furnace was cut. The quartz tubes were removed from the furnace when cool, and the MgO crystals extracted. Any powder adhered to the crystal target surfaces was brushed off before a final polish with 5000 grit paper and/or colloidal silica. To confirm that the single-crystal targets attained the desired atomic proportions of Mg and Fe, we verified their compositions by collecting multiple scanning electron microscopy–energy-dispersive X-ray spectroscopy (SEM–EDS) spot analyses on the target surfaces and edges. (Supplementary Figure 1).

Target composition	MgO	FeO
(0.98Mg, 0.02Fe)	1.44735 g ±0.0001 g	0.052651 ±0.0004 g
(0.95Mg, 0.05Fe)	1.37135 g ±0.0001 g	0.12865 g ±0.0001 g

Supplementary Table 1 The masses of the MgO and FeO powders in grams to generate the target compositions of $(Mg_{0.98},Fe_{0.02})O$ and $(Mg_{0.95},Fe_{0.05})O$.

2 Reflectivity and temperature models

We estimate the reflectivity of (Mg,Fe)O using quartz as a reference. We use the model described in previous work [1], where the quartz reflectivity R_Q is described as

$$R_Q = 4.614 \times 10^{-3} + \frac{(0.3073 - 4.614 \times 10^{-3})U_{S,Q}^{9.730}}{U_{S,Q}^{9.730} + 16.185^{9.730}}. \quad (1)$$

For the temperature measurements, we assume a grey body model, where the emissivity ε ($= 1 - R$, where R is the reflectivity) is independent of wavelength. The temperature T is modeled by [1]

$$T = \frac{T_0}{\ln(1 + (1 - R)\frac{A}{I})}, \quad (2)$$

where T_0(= 1.91eV for quartz) and A are constant and I is the SOP count. We estimate the temperature of (Mg,Fe)O using quartz as a reference.

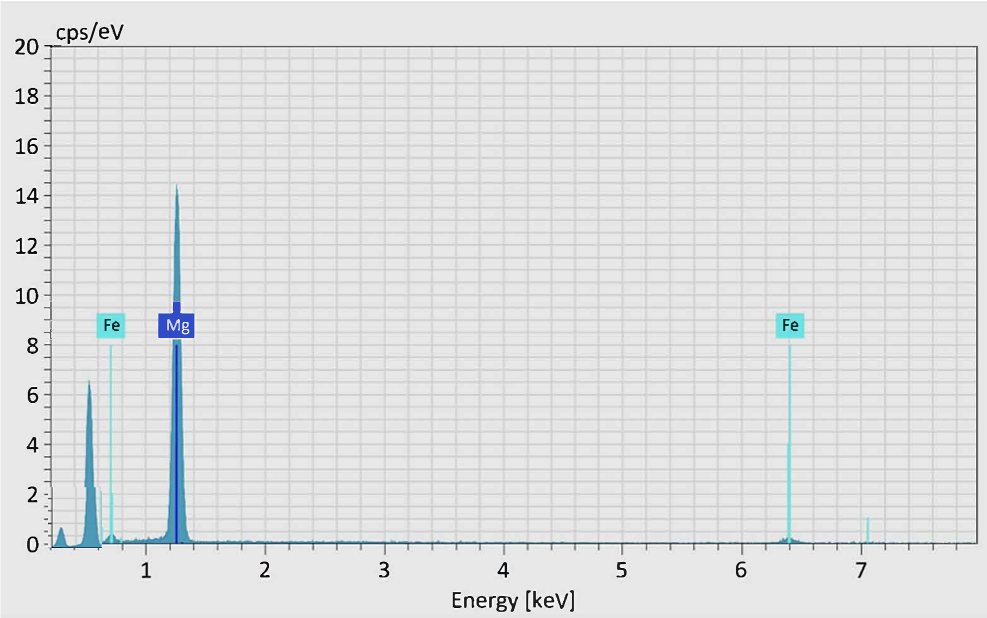

Supplementary Figure 1 Example of a target edge analysis. The relative atomic percent Mg and Fe of a post-interdiffusion MgO target was obtained by combined scanning electron and energy dispersive x-ray spectroscopies (SEM-EDS). Peak characteristics indicate Mg and Fe are the only significant major cations present from multi-point target surface analyses, and translate to $Mg_{94.8}$ and $Fe_{5.2}$, which is close to one of the desired target compositions (($Mg_{0.95}$,$Fe_{0.05}$)O).

3 Additional fit parameters

As shown in the black line in Figure 2a of the main text, the $U_p - u_s$ relationship is described as a linear relationship,

$$U_s = a_s u_p + b_s, \tag{3}$$

where $a_s = 1.23011 \pm 0.00967$ and $b_s = 7.12744 \pm 0.11380$ km s^{-1} based on this work and previously published data. The density and pressure relationship (Figure 2a of the main text) is written as

$$P = a_\rho \rho^2 + b_\rho \rho + c_\rho, \tag{4}$$

where P is the pressure in GPa, and ρ is in g cm^{-3}. Here, a_ρ, b_ρ, c_ρ = 105.98$\pm$ 13 (GPa g^{-2}cm^{-6}), -1168.5 $\pm$ 199 (GPa g^{-1}cm^{-3}), 3532.3 $\pm$ 763 (GPa).

The grey fit in Figure 3b of the main text is described as

$$T(K) = a_T U_S^2 + b_T U_S + c_T, \tag{5}$$

where U_s is in km s^{-1} and $a_T = 426.75 \pm 14.514$ (K s^2 km^{-2}) , $b_T = -14158 \pm 599$ (K s km^{-1}), $c_T = 131180 \pm 6132$ (K). This fit is shown in the grey solid line in the figure.

In Figure 3c of the main text, we show the electrical conductivity estimates from the previous DFT-MD work [2], which is described as

$$\log_{10} \sigma_{\mathrm{H}}(X_{\mathrm{Fe}}) = \log_{10} \sigma_{\mathrm{H}}(0.25) + 16(X_{\mathrm{Fe}} - 0.25), \tag{6}$$

$$\sigma_{\mathrm{H}}(0.25) = \sigma_{\mathrm{H0}} \exp^{-(\Delta E_{\mathrm{H}} + P\Delta V_{\mathrm{H}})/RT}, \tag{7}$$

where σ_{H} is the estimate of the electrical conductivity of (Mg,Fe)O [2], X_{Fe} = Fe/(Fe + Mg) is the iron concentration. The parameters for the Arrhenius type model in Equation 7 are $\sigma_{\mathrm{H0}} = 1.99 \times 10^5$ S m^{-1}, $\Delta E_{\mathrm{H}} = 75.94$ kJ mol^{-1}, $\Delta V_{\mathrm{H}} = -6.1 \times 10^{-8}$ m^3 mol^{-1}. These equations predict the electrical conductivity of 12-20 Sm^{-1} for MgO and 77-132 Sm^{-1} for $(Mg_{0.95},Fe_{0.05})O$, and $1.2 - 2.1 \times 10^5$ Sm^{-1} in the pressure range shown here. Supplementary Figure 2 shows the Z values for the electrical conductivity model (Figure 3c of the main text). Supplementary Figure 3 shows the fit to the d.c. conductivity estimates (Equation 2 in the main text).

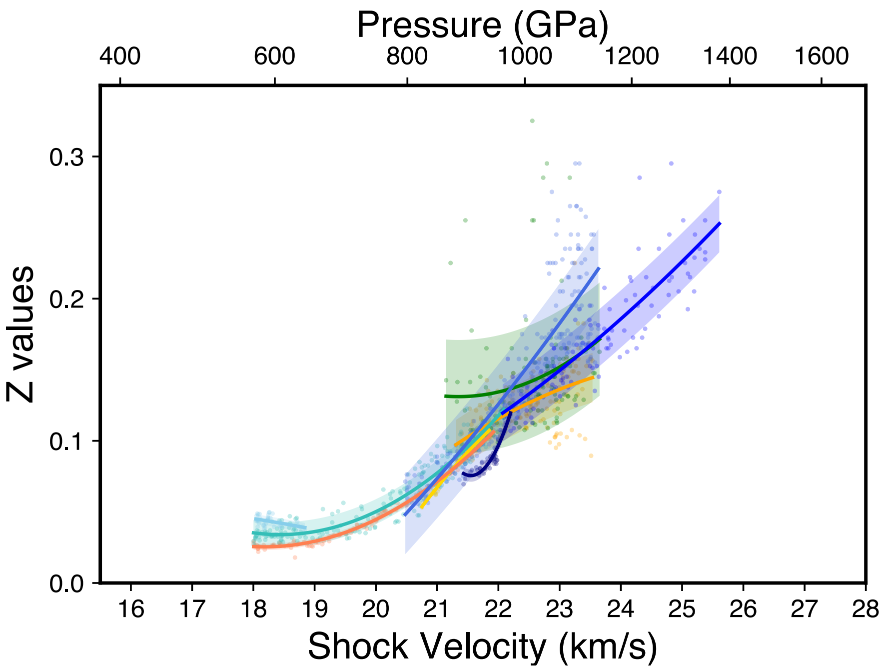

Supplementary Figure 2 Z values used to calculate the d.c. conductivity. The solid lines show the mean and the shaded regions represent ± 1 standard deviation. The corresponding d.c. conductivity is shown in Figure 3c of the main text.

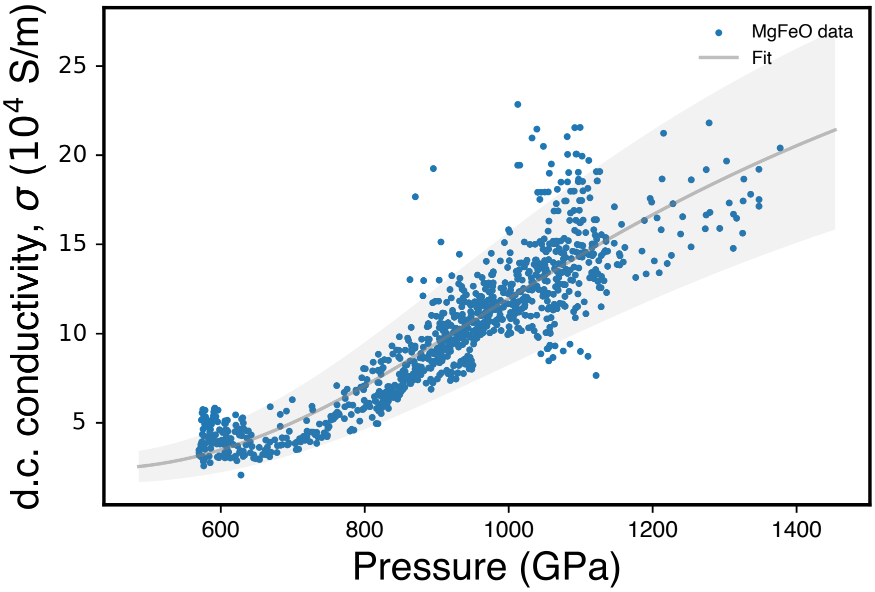

Supplementary Figure 3 The relationship between the pressure and d.c. conductivity. The blue dots represent all of our shock experiment data. The solid grey line represents the best fit to the data (Equation 2 of the main text) and the shaded region represent ± 1 standard deviation.

4 The thermal profiles of the mantle and core

The temperature and pressure conditions at the CMB in our thermal evolution model are shown in Supplementary Figure 4. The average BMO temperatures and pressures are shown in Supplementary Figure 5.

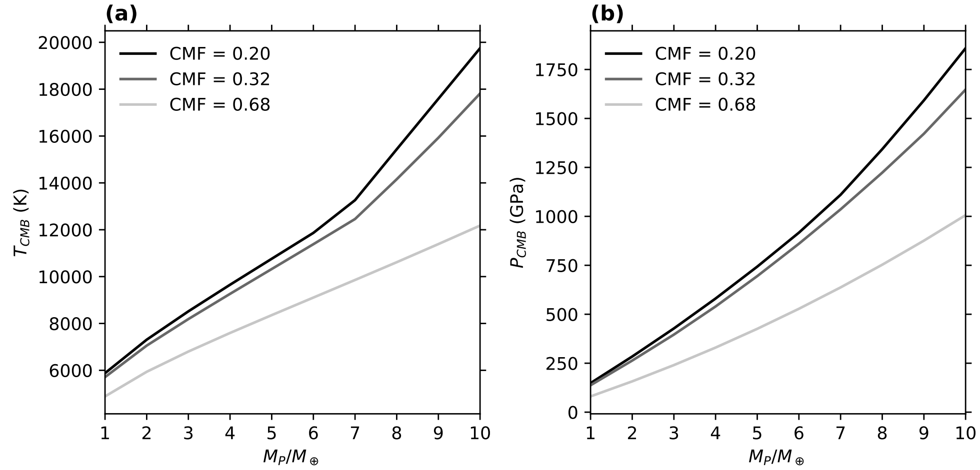

Supplementary Figure 4 The planetary interior conditions at the CMB. (a) Temperature and (b) pressure at the CMB as functions of planetary mass from our thermal evolution model.

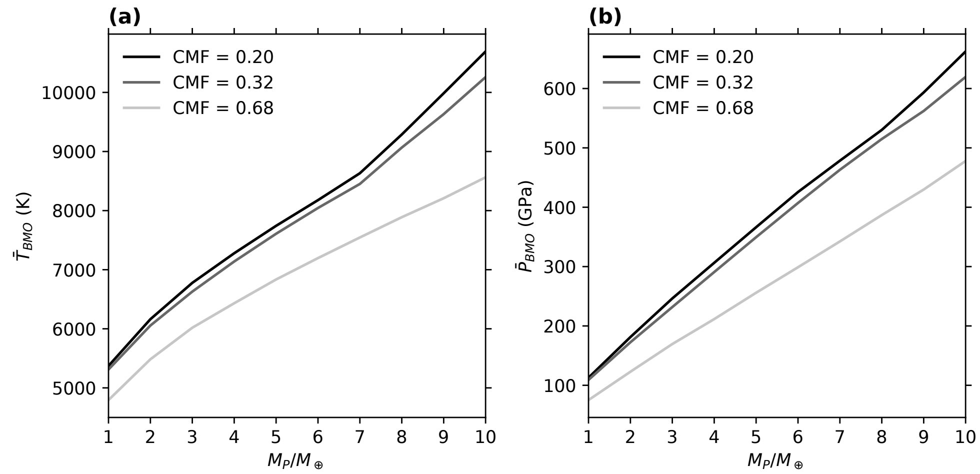

Supplementary Figure 5 The planetary interior conditions at the BMO. (a) The average BMO temperatures (b) and pressures as functions of planetary mass from our thermal evolution model.

5 Radiogenic heating in the core

In our model, we assume that the cores of super-Earths have similar concentrations of radiogenic elements to those of Earth. However, super-Earths may have higher concentrations if their metal-silicate partition coefficients under high pressures are high. Luo et al. [3] propose such a scenario in which the super-Earth core has high concentrations of potassium, thorium, and uranium, producing a large heat flux from the core.

Here, we investigate its potential effect; we vary the potassium concentration from 10^{-1} to 860 ppm in a 6 $M_{\oplus}$ super-Earth with the core mass fraction of 0.32. These potassium concentrations correspond to $\sim 0.012 - 101$ ppb of ^{40}K in the core. We do not have uranium or thorium in our model. Supplementary Figure 6 shows the evolution of the entropy of dissipation, magnetic Reynolds number, and surface magnetic field strength over time. As can be seen in the figure, the concentration of potassium does not change the evolution in a significant way. The same argument holds for the minimum electrical conductivity required for a BMO-driven dynamo (Supplementary Figure 7).

Higher concentration of potassium is possible, but we are unable to simulate it with our current model, as such a high potassium concentration can lead to melting the whole mantle and forming the whole magma ocean instead of a basal magma ocean, breaking the primary assumption of our model. The high concentrations of heat-producing elements in the super-Earth's core are certainly an interesting idea and worth exploration, but it should be noted that the concentrations are highly uncertain given that we still do not know these abundances in Earth's core in detail [4]. It would be important to investigate their metal-silicate partition coefficients in high pressure experiments in order to test the results from the ab initio molecular dynamics simulations by Luo et al. [3].

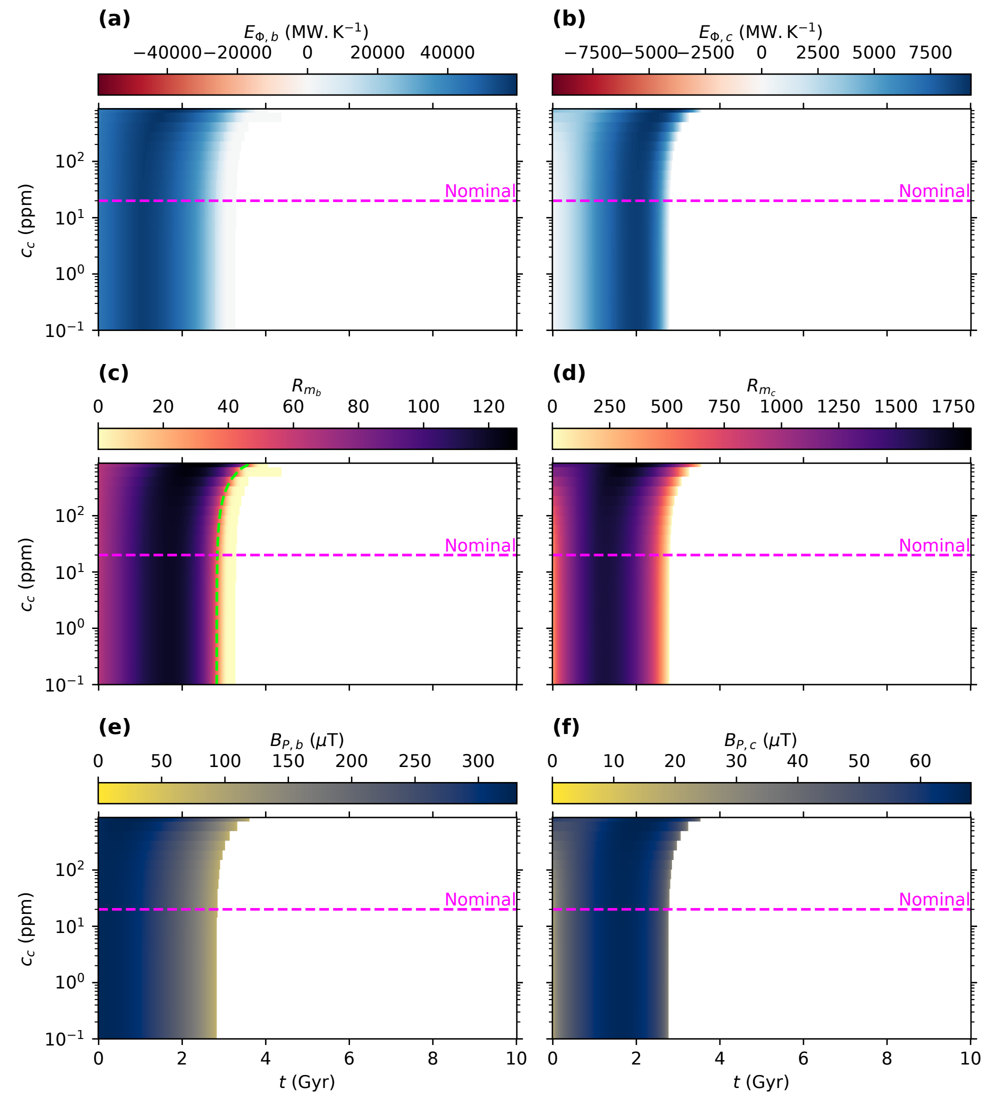

Supplementary Figure 6 Time evolution of (a,b) the entropy of dissipation E_ϕ, (c,d) magnetic Reynolds number R_m, and (e,f) surface magnetic field strength B_P as a function of time in Gyr. The $y-$axis c_c is the potassium concentration in ppm. The subscript b and c refer to the mantle and core. The purple dashed line represents the nominal Earth-like setting. The Green dashed lines correspond to $E_\phi = 0$ (a,b) and $R_m = 40$ (c,d) as the criteria for dynamo generation. The planetary mass is 6 $M_\oplus$ and the core mass fraction (CMF=0.32).

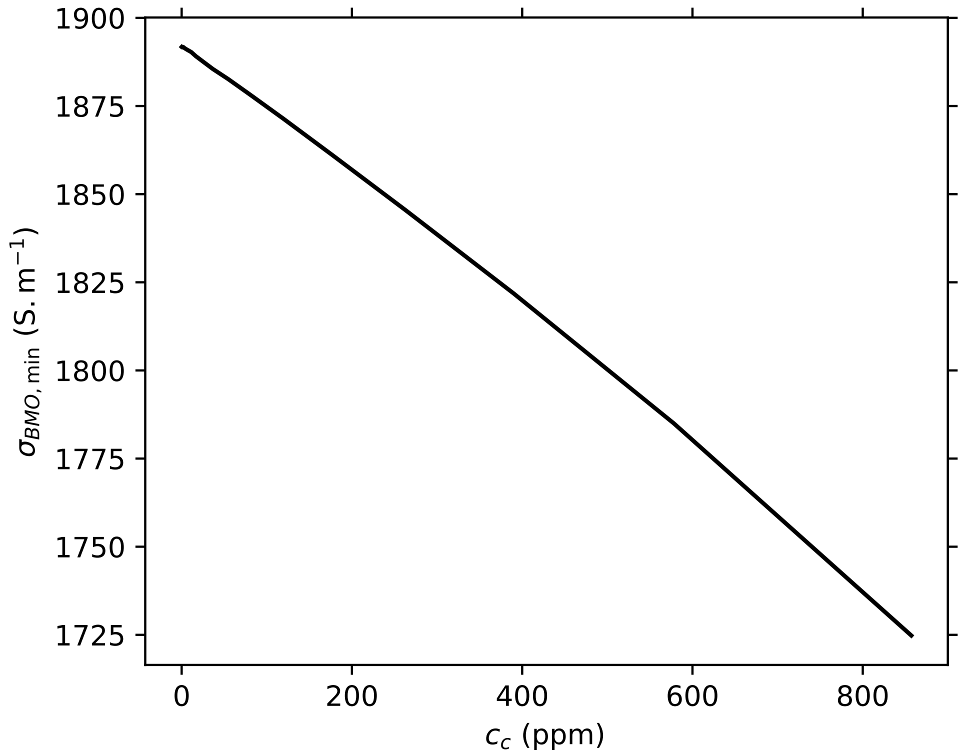

Supplementary Figure 7 The minimum electrical conductivity required for a BMO-driven dynamo as a function of potassium concentration.

References

[1] Millot, M. *et al.* Shock compression of stishovite and melting of silica at planetary interior conditions. *Science* **347**, 418–420 (2015).

[2] Holmström, E., Stixrude, L., Scipioni, R. & Foster, A. S. Electronic conductivity of solid and liquid (mg, fe)o computed from first principles. *Earth Planet. Sci. Lett.* **490**, 11–19 (2018).

[3] Luo, H., O'Rourke, J. G. & Deng, J. Radiogenic heating sustains long-lived volcanism andmagnetic dynamos in super-earths. *Sci. Adv.* **10**, eado7603 (2024).

[4] Nimmo, F. Energetics of the core. *Treatise on Geophysics, Second Edition* 27–55 (2015).